Radiative scaling of the nocturnal boundary layer and the diurnal temperature range

Alan K. Betts[1]

Received 4 August 2005; revised 6 December 2005; accepted 18 January 2006; published 7 April 2006.

[1] A radiative scaling for the warm season nocturnal boundary layer (NBL) is proposed, based on the daily mean surface net longwave radiation flux. Using this scaling, a conceptual model is proposed for the NBL, with parameters estimated from multiple linear regression of model data from the European Centre reanalysis, averaged over river basins from the tropics to high latitudes. A radiative temperature scale, computed from surface net longwave radiation flux and the slope of the Stefan-Boltzmann law, primarily determines the strength of the NBL and the amplitude of the diurnal temperature range, although the length of the nighttime period and the surface wind stress play important subsidiary roles. A related radiative velocity scale or radiative conductance, the duration of the nighttime period and the ratio of the scaled surface heat flux (which increases with wind stress) to the NBL strength determine the depth of the NBL. From an observational perspective, this suggests that the diurnal temperature range may give a useful estimate of surface net longwave radiation flux. From a modeling perspective, this provides a framework for relating model physical parameterizations, especially the coupling at night between the surface, the ground and the atmosphere, to observables, the diurnal temperature range and the strength and depth of the NBL. The model is then applied to estimate the nocturnal rise in concentration of gases such as CO_2 and radon that are emitted at the surface.

Citation: Betts, A. K. (2006), Radiative scaling of the nocturnal boundary layer and the diurnal temperature range, *J. Geophys. Res.*, *111*, D07105, doi:10.1029/2005JD006560.

1. Introduction

[2] This paper proposes a radiative scaling for the nocturnal boundary layer (NBL) over land, based on the 24-h mean surface net longwave radiation flux (LW_{net24}). The same radiative scaling is also applied to the diurnal temperature range (DTR), an important climate parameter. Worldwide, the DTR has been decreasing in recent decades [*Karl et al.*, 1993; *Horton*, 1995; *Easterling et al.*, 1997]. Coincident increases of cloud cover, which would reduce outgoing LW_{net}, have been noted by many authors [e.g., *Henderson-Sellers*, 1992; *Dessens and Bucher*, 1995; *Jones*, 1995]. Indeed, the analysis of *Dai et al.* [1999] provides evidence of the close coupling of cloud cover with DTR.

[3] There has been extensive development of similarity theory for the stable boundary layer (BL), but the role of radiative cooling is generally not considered in this scaling [e.g., *Nieuwstadt*, 1984; *Derbyshire*, 1994; *Stull*, 1988]. A nighttime surface energy balance model was developed by *Holtslag and De Bruin* [1988], in which the so-called isothermal net radiation [*Monteith*, 1981] plays an important role. Over land, however, the diurnal cycle is driven by daytime radiative heating and the nocturnal longwave cooling of the surface [e.g., *Betts*, 2003]. The development of mixed layer models were a major breakthrough in understanding the unstable daytime dry and cumulus BLs [*Deardorff et al.*, 1969; *Betts*, 1973; *Carson*, 1973; *Tennekes*, 1973], as well as mixed stratocumulus layers [*Lilly*, 1968]. These recognized the role of the radiative forcing at the surface and at cloud-top in generating the turbulence, which produces nearly well-mixed layers. Surprisingly, comparatively little attention has been paid to the corresponding role of radiative forcing in determining the strength and depth of the NBL; so this is the focus of this paper. Conceptually, it is a different starting point from the traditional wind and stability framework, although we will show that wind stress remains a significant independent factor, as it affects the coupling between surface and atmosphere. This analysis will show that the strength of the NBL at sunrise (which will be defined later in section 2.3, equation (5a) as a temperature difference, ΔT_N) and the DTR are directly related to a radiative temperature scale, associated with the slope of the Stefan-Boltzmann equation. We start using the framework of model data from the European Centre for Medium-range Forecasts (ECMWF) reanalysis (known as ERA-40 [*Uppala et al.*, 2005]) to illustrate the scaling, and quantify relationships using multiple linear regression. In the model data, after scaling, ΔT_N and DTR increase with the growth-time of the NBL and decrease weakly with increasing wind stress. A conceptual

[1]Atmospheric Research, Pittsford, Vermont, USA.

0148-0227/06/2005JD006560$09.00

Table 1. ERA-40 River Basins

River Subbasins	ERA-40 ID	Latitude, Longitude (Mean)
Arkansas-Red	28	35.9°N 109.8°W
Missouri	29	43.6°N 113.1°W
Upper Mississippi	30	43.1°N 102.3°W
Ohio	31	38.1°N 94.8°W
Lower Mississippi	32	34.9°N 101.5°W
Peel	33	66.8°N 144.1°W
Great Bear Lake	34	64.5°N 133.8°W
Great Slave Lake	35	61.4°N 124.7°W
Liard	36	60.0°N 134.6°W
Peace (East)	37	58.2°N 122.3°W
Peace (West)	38	56.2°N 132.8°W
Athabasca	39	56.4°N 121.2°W
La Plata	40	24.1°S 69.5°W
Tapajos/Xingu	41	7.0°S 67.8°W
Madeira	42	13.0°S 75.4°W
Amazonas	43	5.1°S 84.0°W
Negro	44	0.1°S 74.9°W
Jurua/Purus	45	6.8°S 79.5°W

model for the depth, **h**, of the NBL is then developed in terms of a radiative velocity scale, and the scaled surface heat flux which increases steeply with wind stress. This simple model is then applied to estimate the nocturnal rise in concentration of gases such as CO_2 and radon that are emitted at the surface and trapped within the NBL.

[4] Modeling the stable boundary layer (BL) has presented considerable difficulties in global models. In the ECMWF model, the stable BL was reformulated [*Viterbo et al.*, 1999] to reduce cold temperature biases in winter over continental areas. Changing the stability functions introduced more diffusion at high stable Richardson numbers, which in turn increased the coupling between surface and atmosphere, and reduced the fall of surface temperature at night, driven by radiative cooling. However, more diffusion gives deeper stable BLs, which may now be too deep in the model (Beljaars, 2005, personal communication). *Viterbo et al.* [1999] also addressed the effect of the thermal inertia of soil freezing in damping the response of the surface temperature in winter. The ERA-40 reanalysis model uses this same formulation of the stable BL (documentation is available at http://www.ecmwf.int/research/ifsdocs/CY23r4/index.html), although the model data presented here will be for the warm season. Since this analysis is based entirely on model output data, our conclusions do depend on the model physics parameterizations, particularly the stable BL and ground heat flux parameterizations. The model data we use is averaged over river basins (see next section). This smooths and simplifies the analysis, but this means that the evaluation of our results against observations is not an easy task, and it is left to future work.

2. Scaling of Mean Diurnal Cycle

[5] Model data can provide powerful insights into the coupling of physical processes, even though quantitatively there will be dependence on a given model's specific parameterizations. The ERA-40 archive [*Kållberg et al.*, 2004] contains hourly data averaged over river basins. These were originally archived to study the hydrometeorology of river basins [see *Betts et al.*, 2003, 2005]. In other papers [*Betts*, 2004; *Betts and Viterbo*, 2005] these data have been used to explore the interrelation of the surface fluxes, the BL, the cloud fields and surface radiation balance on the daily timescale. *Betts* [2004] showed one example of the relationship of the DTR to the diurnally averaged surface net longwave radiation flux for the Madeira River. This analysis of the DTR is extended here to include other river basins across the Americas, and adapted to address the radiative scaling of the NBL. Table 1 identifies the subbasins of the Mackenzie, Mississippi, Amazon and La Plata rivers and their approximate latitude and longitude. The data period we have chosen for analysis is a seven-year period, 1993–1999. The model data are used in two forms. In this section, the monthly mean diurnal cycle is presented to illustrate the radiative scaling of the diurnal cycle. In section 3, parameters are extracted for each day to relate the strength of the NBL, the DTR and the surface heat flux to the surface net longwave radiation flux.

2.1. Mean Diurnal Cycle

[6] Figure 1a shows the mean diurnal cycle of 2-m temperature (T_2) for the Madeira River basin for four months. January and February are in the heart of the rainy season, and both show a small amplitude diurnal cycle of temperature. Six months later, July and August are in the dry season, and the diurnal temperature range

$$\mathrm{DTR} = \mathrm{T_{max}} - \mathrm{T_{min}} \tag{1}$$

(where T_{max}, T_{min} are the maximum and minimum values of T_2) has about twice the amplitude. For this Amazon basin, sunrise is around 1030 UTC; slightly later in July and August, as the basin is south of the equator). Figure1b shows that the surface LW_{net} has a similar increase from wet to dry season. Since the NBL is created by net long-wave cooling of the surface at night, the stronger the outgoing LW_{net}, the greater the cooling of the surface, and the larger the amplitude of the diurnal temperature cycle [*Betts*, 2004]. In the dry season, the atmospheric water vapor and cloud cover are reduced, and the lifting condensation level (LCL) is higher, and all these factors contribute to a greater outgoing LW_{net} [*Betts and Viterbo*, 2005].

2.2. Radiative Temperature Scale

[7] *Betts* [2004] showed that the diurnal temperature range was related to the 24-h mean net longwave radiation flux, LW_{net24}, and to a related radiative temperature scale, defined as

$$\Delta \mathrm{T_R} = -\lambda_0 \ \mathrm{LW_{net24}} \tag{2}$$

where $\lambda_0 = 1/(4\sigma T^3)$ is the radiative sensitivity parameter from the differential of the Stefan-Boltzmann law, in which $\sigma = 5.67\ 10^{-8}$ W m^{-2} K^{-4} is the Stefan-Boltzmann constant. At T = 293 K, $4\sigma T^3 = 5.7$ Wm^{-2} K^{-1}, giving $\lambda_0 = 0.175$ K/(Wm^{-2}).

2.3. Scaled Diurnal Cycle

[8] The radiative temperature scale (2) can be used to scale the diurnal cycle of temperature, by defining a scaled temperature perturbation from the 24-h mean temperature, T_{24}, as

$$\mathrm{T_{sc}} = (\mathrm{T_2} - \mathrm{T_{24}})/\Delta \mathrm{T_R} \tag{3}$$

Figure 2 shows that the transformation from T_2 to T_{sc} collapses the widely different diurnal temperature cycles

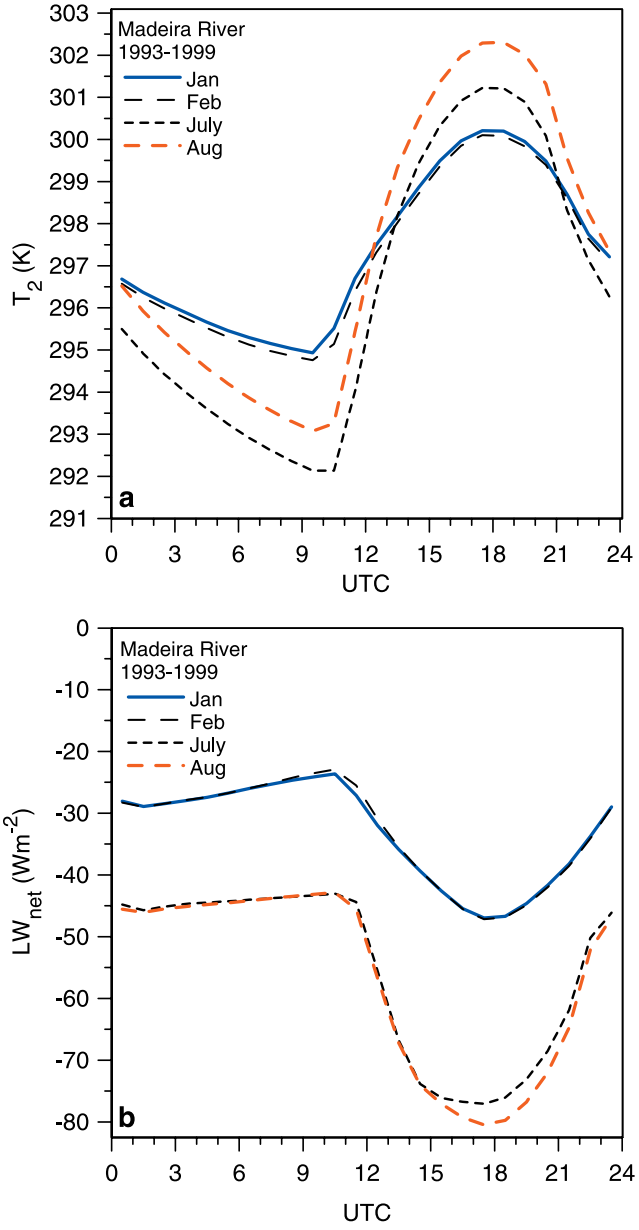

Figure 1. Mean diurnal cycle for Madeira River basin of (a) 2-m temperature and (b) surface net longwave radiation flux.

shown in Figure 1a into almost a single curve. The scaled amplitude of the diurnal temperature cycle is defined as

$$DTR_{sc} = T_{maxsc} - T_{minsc} \quad (4)$$

For this tropical basin, $DTR_{sc} \approx 1$.

[9] The diurnal cycle of the sensible heat flux, H, for the same four months is also shown in Figure 2 (right-hand-scale). In the late afternoon or evening, temperature falls from T_{maxsc} as H falls. For the purpose of this paper, the NBL is defined as the period when $H < 0$. The NBL starts growing, when H first becomes negative at an unscaled temperature, T_N, corresponding to the scaled temperature T_{Nsc} shown. At this point, the potential temperature gradient near the surface is neutral, as the transition occurs from an unstable to a stable BL. To get a better estimate of T_{Nsc}, adjacent hours were interpolated linearly to give the value of T_{sc} at H = 0. The NBL reaches its maximum strength at sunrise, when $T_{sc} = T_{minsc}$ (and $T_2 = T_{min}$). The NBL is growing during the period between the vertical dotted line near 2000 UTC, and the dotted line at the morning temperature minimum. For this paper, the strength of the NBL at sunrise is defined as the difference in surface temperature from the initial formation of the NBL, in unscaled units

$$\Delta T_N = T_N - T_{min} \quad (5a)$$

and in scaled units

$$\Delta T_{Nsc} = T_{Nsc} - T_{minsc} \quad (5b)$$

Only the ERA-40 surface parameters are analyzed in this paper, and simple vertical profiles for the NBL will be assumed for energy balance calculations in section 4. The analysis of the ERA-40 vertical profile data is a much larger task (we have years of hourly data for 18 basins), which will be attempted later.

2.4. Scaled Temperature Diurnal Cycle Across Different River Basins

[10] Figure 3 shows the scaled diurnal temperature cycle across the set of river basins. The location of the river basins is shown in Figure 7 of *Betts* [2004].The Amazon basins in Figure 3a are very similar, have the largest amplitude, and very little seasonal variation (not shown). For the La Plata (which is a single basin in the ERA-40 archive), the amplitude is a little smaller and decreases further in the austral winter, which is rather mild at this latitude. For the Mississippi subbasins, a summer average from May to August is shown in Figure 3c, and the amplitudes are also smaller, and decrease slightly from the most southern basin (Lower Mississippi) to the Missouri basin. Finally for the high latitude Mackenzie River in Figure 3d, three representative basins are shown. The amplitude of the scaled diurnal cycle decreases still further to the most northern basin shown, Great Bear Lake, which is close to the Arctic circle (see Table 1). We conclude that the scaling by the radiative

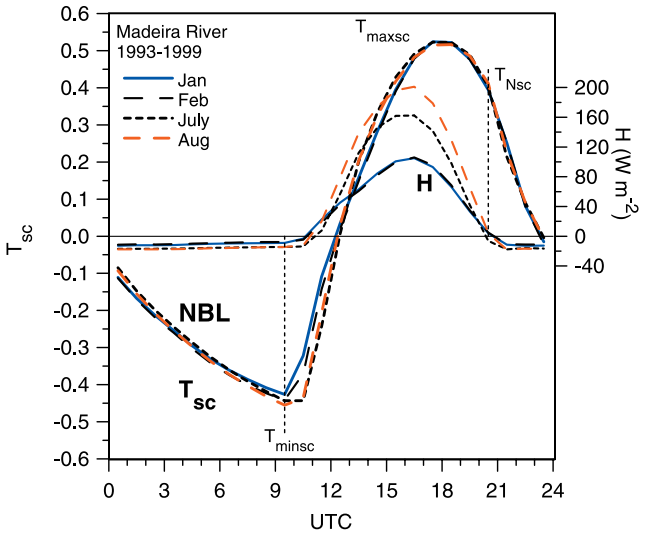

Figure 2. As Figure 1 for scaled 2-m temperature and surface sensible heat flux, H.

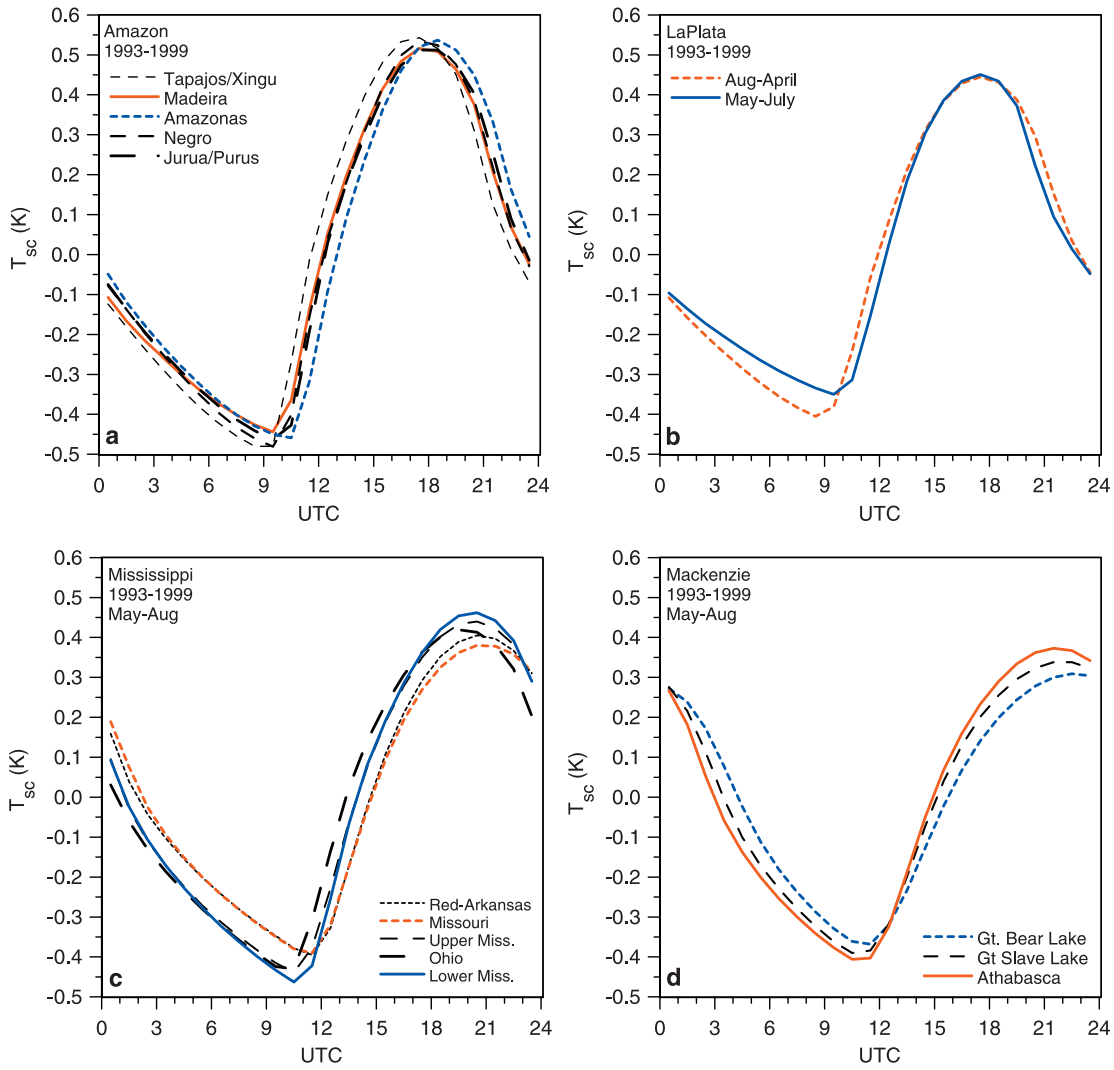

Figure 3. Scaled diurnal cycle of 2-m temperature for selected river basins (a) Amazon, (b) La Plata, (c) Mississippi, (d) Mackenzie.

temperature (2) appears to be useful across a wide range of latitudes and climates. However, the scaled amplitude decreases as latitude increases and night-length decreases. This will be explored further using daily data in section 3.2.

2.5. Scaled Surface Energy Balance

[11] The surface energy balance is

$$SW_{net} + LW_{net} = \lambda E + H + G \quad (6)$$

where SW_{net}, λE and G are the surface net shortwave flux, latent heat flux and ground flux respectively. For the NBL period when $H < 0$, $SW_{net} \approx \lambda E$ and both are small (SW_{net} is not identically zero, because H becomes <0 before sunset). This leaves the approximate energy balance for the NBL period

$$LW_{netN} \approx H_N + G_N \quad (7)$$

The sign convention is that all terms in (7) are negative. This partition of the outgoing LW_{netN} energy loss into fluxes from the atmosphere and the ground does depend on the model parameterizations for the stable BL and the ground heat flux. It also depends on wind stress (see section 3.3, later).

[12] Scaling by $-LW_{net24}$ (for consistency with equation (2)) gives

$$H_{Nsc} + G_{Nsc} \approx LW_{netN}/LW_{net24} \quad (8)$$

where both the scaled NBL sensible heat flux and ground heat flux are now defined positive. The ratio $LW_{netN}/LW_{net24} \approx 0.75$ for these data.

3. Model Parameters From Daily ERA-40 Surface Data

[13] Parameters are extracted for each basin for each day in the period 1993–1999 to study the relationship of the amplitude of the diurnal cycle, the strength of the NBL and of the nighttime surface heat flux to the surface longwave cooling, NBL growth time, surface wind stress. The original model hourly data used are from single 24-h forecasts from each 0000 UTC analysis, so there can be a small disconti-

nuity at 0000 UTC time, as the originating analysis changes, but this factor was ignored. The three temperatures, T_{max}, T_N and T_{min} were found, as outlined in the discussion of Figure 2, for each 24-h time period starting at 1500 UTC (corresponding to roughly mid-morning for these basins in the Americas). From (1) and (5a), these define the DTR and ΔT_N. Using equations (2), (3), (4) and (5b), the scaled amplitudes DTR_{sc} and ΔT_{Nsc} were then calculated for each 24-h period. For the NBL period (defined again as the hours when $H < 0$), the mean values of H_N, and the other surface fluxes including the surface stress, were computed, as well as the mean 10-m wind-speed, V_{10N}. The growth time of the NBL, τ_N, was computed by subtracting the time at T_{min} from the earlier time at T_N, found by linear interpolation to where $H = 0$. Only a few percent of the days were rejected from the analysis if they showed a temporal structure grossly inconsistent with Figure 2, often due to large temperature advection during the 24-h period.

3.1. Diurnal Temperature Range Dependence on ΔT_R

[14] Figure 4shows the dependence of the DTR on ΔT_R for two basins of the Amazon, which have a large seasonal cycle, and the summer data (June, July and August) for the subbasins of the Mackenzie, together with the regression lines through the origin. For the Amazon the regression line slope is close to 1, which is consistent with Figure 3a, and correlation is quite high ($R^2 = 0.84$). For the Mackenzie, the slope is smaller, only 0.73, consistent with Figure 3d, and the correlation is weaker ($R^2 = 0.59$). The basins of the Mississippi and the LaPlata (not shown) lie in between these two extremes. The corresponding plots for the dependence of ΔT_N on ΔT_R are very similar with smaller slopes, so it is clearly useful to explore the dependencies of the scaled amplitudes DTR_{sc} and ΔT_{Nsc} on other variables. The regression coefficients are higher using LW_{net24} to calculate ΔT_R in (2), than if LW_{netN} were used (not shown).

3.2. Dependence of DTR_{sc} and ΔT_{Nsc} on NBL Growth Time, τ_N

[15] One factor affecting the decrease of DTR_{sc} from the tropics to the high latitudes is the decreasing nighttime period in summer for the development of the NBL. To show this, we binned all the daily data (in 0.1 ranges of τ_N) from the warm season, the months June-August for the Mackenzie, May to August for the Mississippi and the corresponding months November-February for the southern hemisphere La Plata basin, together with 12 months of data from the two Amazon basins with the largest seasonal cycle (basin 42 the Madeira, and 41 the Tapajos/Xingu, see Table 1), a total of 13731 days of model data. Figure 5 shows that in the mean the scaled diurnal temperature range DTR_{sc} and strength of the NBL ΔT_{Nsc} increase together with the duration of the NBL growth time, τ_N. For the most northern basins of the Mackenzie, $\tau_N \approx 9$ h in summer, and $DTR_{sc} \approx 0.7$; while for the Amazon basins, $\tau_N \approx 13.5$ h, and $DTR_{sc} \approx 1.02$, consistent with Figures 3 and 4. ΔT_{Nsc} is systematically lower than DTR_{sc}, with the mean ratio of $\Delta T_{Nsc}/DTR_{sc} = 0.90 \pm 0.07$ for this set of days.

3.3. Dependence on Surface Stress and Surface Wind

[16] Another factor affecting DTR_{sc}, ΔT_{Nsc} and the NBL heat flux, H_{Nsc} is the strength of the coupling between the surface and the atmosphere, which will be represented here by the surface friction velocity. For the same data set of 13731 warm season days, Figure 6a shows the dependence of the NBL 10-m wind, V_{10N}, in the model on the NBL friction velocity, defined as

$$U_{starN} = (StressN/\rho)^{0.5} \quad (9)$$

where StressN is the mean surface stress for the NBL period and ρ the corresponding mean density. Not surprisingly there is a quasi-linear relationship. The variability depends on the surface roughness, which at each gridpoint in the model has a local component, depending on vegetation

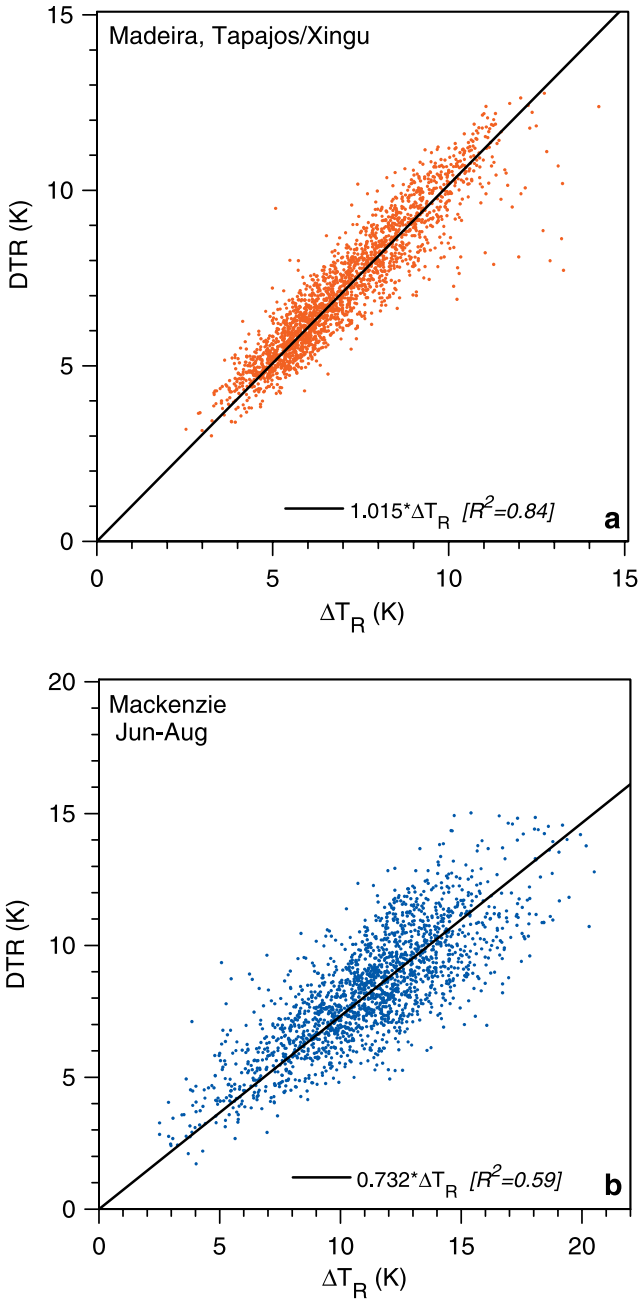

Figure 4. (a) DTR plotted against radiative temperature scale for two Amazon basins. (b) As Figure 4a for Mackenzie subbasins in summer.

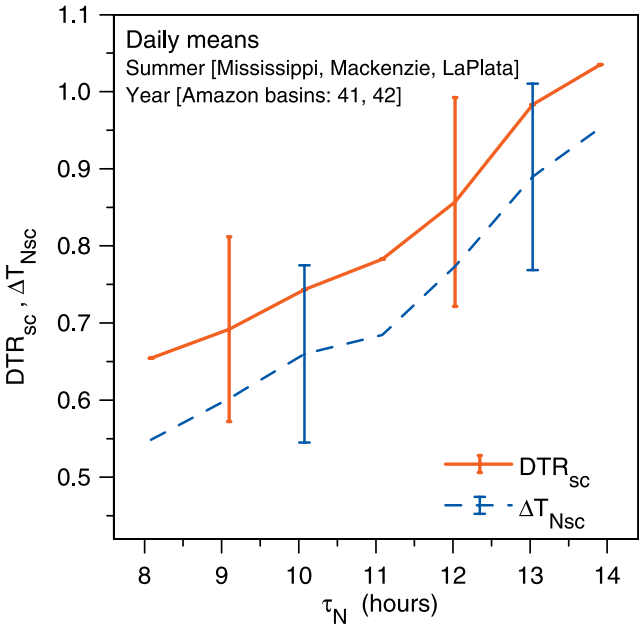

Figure 5. Variation of DTR_{sc} and NBL ΔT_{Nsc} with τ_N (with representative standard deviations).

type, and an orographic component; and in addition a stability dependence through the model surface layer parameterization. Thus, V_{10N} has a strong dependence on the model parameterizations, and the data will be stratified by NBL friction velocity (related to wind stress), rather than wind-speed. In fact, the multiple linear regression correlation, discussed in the next section, is higher with U_{starN} as an independent variable than with V_{10N}.

[17] Figure 6b shows the dependence of DTR_{sc} (top right-hand-scale), ΔT_{Nsc} and the NBL heat flux, H_{Nsc} on U_{starN} and τ_N, for three values of τ_N, together with representative standard deviations. Only $\tau_N = 12$h has sufficient data in the highest U_{starN} class. DTR_{sc} and ΔT_{Nsc} both increase with τ_N, as shown in Figure 5, and decrease slowly with increasing friction velocity (and windspeed). In contrast, the scaled surface heat flux, H_{Nsc}, has almost no dependence on τ_N, but increases steeply with friction velocity, as the coupling between surface and atmosphere increases. The corresponding ground storage flux, G_{Nsc}, in equation (8) decreases with increasing U_{starN} (not shown).

3.4. Linear Regression Fits

[18] For this same set of 13731 warm season days of model data from the Amazon, LaPlata, Mississippi and Mackenzie basins, multiple linear regression was used to fit ΔT_{Nsc}, DTR_{sc} and H_{Nsc} as functions of τ_N and U_{starN}. This gave

$$DTR_{sc} = 0.984(\pm 0.009) + 0.0675(\pm 0.0007)(\tau_N - 12) - 0.425(\pm 0.011)U_{starN} \quad (R^2 = 0.49) \quad (10)$$

$$\Delta T_{Nsc} = 0.902(\pm 0.008) + 0.0701(\pm 0.0006)(\tau_N - 12) - 0.451(\pm 0.009)U_{starN} \quad (R^2 = 0.56) \quad (11)$$

$$H_{Nsc} = 0.037(\pm 0.006) + 0.0120(\pm 0.0005)(\tau_N - 12) + 1.135(\pm 0.007)U_{starN} \quad (R^2 = 0.63) \quad (12)$$

The R^2 coefficient is higher for H_{sc} than for ΔT_{Nsc} and DTR_{sc}.

[19] Figure 7 shows the structure of these linear fits. The dependence on τ_N is greater for ΔT_{Nsc} and DTR_{sc} than for H_{Nsc}, and the reverse is true for the dependence on U_{starN}. Note the close similarity (for regions where there was data) to Figure 6b, which is plotted with identical scales. These regression fits from model data, shown in Figure 7, will be used in the next section as input to our simple model. As mentioned earlier, U_{starN} as an independent variable gives higher regression coefficients than using windspeed V_{10N}. The scaling by LW_{net24}, rather than LW_{netN}, gives higher regression coefficients for DTR_{sc} and ΔT_{Nsc} but not for the nighttime flux H_{Nsc}.

4. Conceptual Model for the NBL

[20] A conceptual model for the NBL, using LW_{net24} as a scaling parameter, is now proposed.

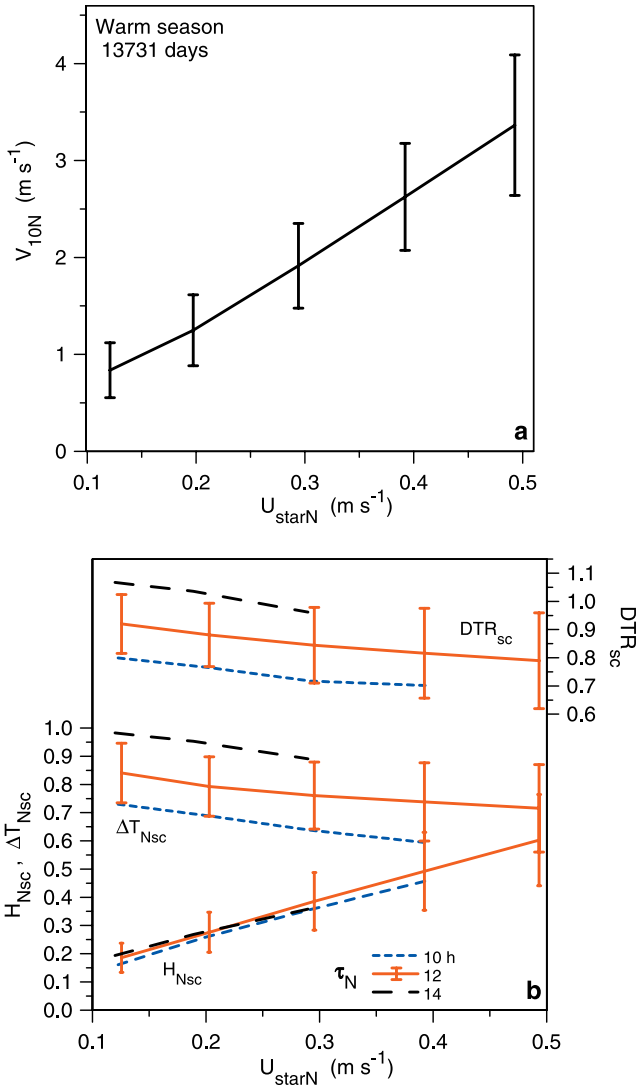

Figure 6. (a) Dependence of V_{10N} on friction velocity. (b) Dependence of DTR_{sc}, ΔT_{Nsc} and H_{Nsc} on friction velocity and τ_N.

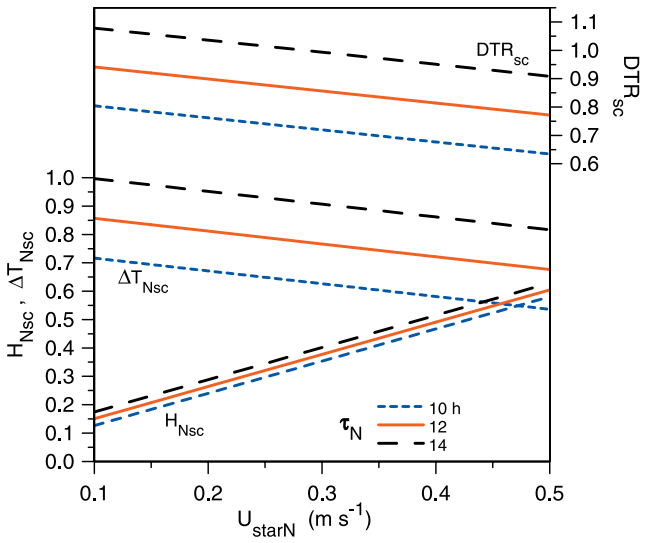

Figure 7. Structure of regression fits for DTR_{sc}, ΔT_{Nsc} and H_{Nsc} as a function of U_{starN} and τ_N.

4.1. Simplified NBL Structure

[21] Figure 8 shows the vertical structure of the conceptual model. After the local temperature maximum, we suppose the daytime mixed layer is exactly neutral (with constant potential temperature, θ) at the moment when H changes sign from positive to negative. At this point the 2-m temperature, T_N, lies on this same dry adiabat. During the nocturnal period, lasting time τ_N, the surface cools and the NBL is created. By dawn, after the nighttime cooling, an NBL has formed with depth **h**, with a surface cooling of $\Delta T_N = T_N - T_{min}$ below the potential temperature of the preceding daytime mixed layer. The temperature profile with height will be assumed: Figure 8 shows the linear and quadratic profile (with $\partial\theta/\partial z = 0$ at height **h**), that will be used. The radiative cooling of the residual mixed layer above **h** will be neglected.

4.2. Energy Balance for the NBL

[22] Integrating over the NBL growth period, τ_N, the heat storage in the NBL satisfies

$$-H_N\,\tau_N = \rho\,C_p\,\beta\,\Delta T_N\,\mathbf{h} \tag{13}$$

where ρ is air density and C_p is the specific heat of air at constant pressure (both assumed constant). The radiative flux divergence within the NBL is an additional term in the energy budget, which will be ignored for simplicity; although it could also be related to the surface LW_{net}. For the linear, quadratic profiles of NBL temperature shown in Figure 8, $\beta = 0.5, 0.333$. Scaling by $-LW_{net24}$ and using (2), (3) and (5b) gives

$$H_{Nsc}\,\tau_N = \rho\,C_p\,\beta\,\lambda_0\,\mathbf{h}\,\Delta T_{Nsc} \tag{14}$$

Rearranging gives the depth of the NBL

$$\mathbf{h} = (H_{Nsc}/\beta\,\Delta T_{Nsc})\mathbf{W_R}\,\tau_N \tag{15}$$

where the radiative velocity scale (or radiative conductance) is given by

$$\mathbf{W_R} = 1/(\rho C_p \lambda_0) \tag{16}$$

At 293K and 1000hPa, $\mathbf{W_R} \approx 0.0048\text{m s}^{-1}$, which is about 40 hPa day^{-1}. Substituting

$$H_{Nsc} \approx \beta \approx 0.5 \text{ and } \Delta T_{Nsc} \approx 1$$

gives

$$\mathbf{h} \approx \mathbf{W_R}\,\tau_N \tag{17}$$

so that with these simple assumptions, a typical NBL depth for $\tau_N \approx 12$ hours is of order 20 hPa or 200m.

[23] More exactly, equation (15) shows that (for constant β) **h** is proportional to the scaled heat flux, H_{sc}, the length of the stable period, τ_N, and inversely to ΔT_{Nsc}. Using equations (11) and (12), the regression fits from the ERA-40 data in Figure 7, as an estimate of these dependencies, (15) can be rearranged as

$$\mathbf{h} = \mathbf{W_R}\,\tau_N/\beta R \tag{18a}$$

where

$$\begin{aligned} R &= (\Delta T_{Nsc}/H_{Nsc}) \\ &= (0.902 + 0.070(\tau_N - 12) - 0.451U_{starN}) \\ &\quad /(0.037 + 0.012(\tau_N - 12) + 1.135U_{starN}) \end{aligned} \tag{18b}$$

Figure 9 shows the structure of the solution of (18a) at 293 K, for both linear and quadratic NBL profiles. NBL depth at sunrise increases steeply with mean nighttime U_{starN}, and has little dependence on NBL duration. Comparing Figures 7 and 9, increasing U_{starN} gives a larger

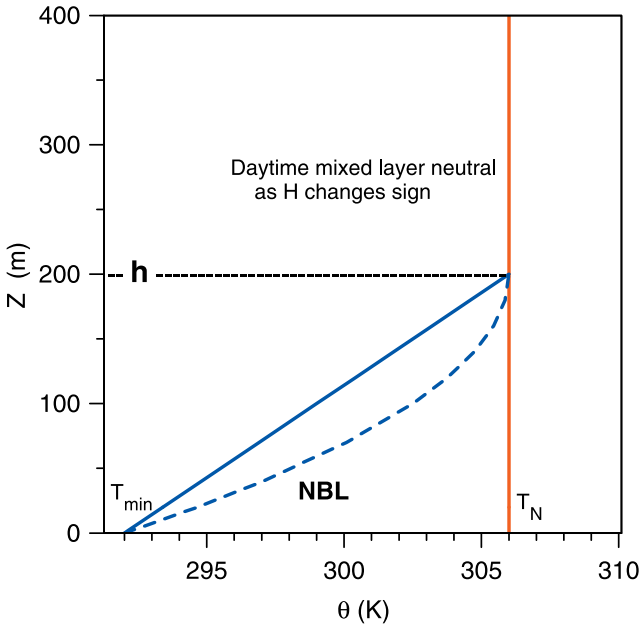

Figure 8. Idealized nocturnal boundary layer structure.

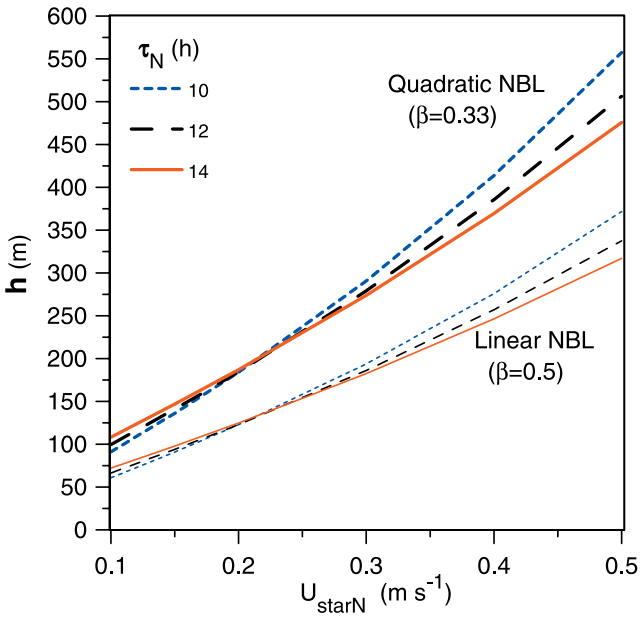

Figure 9. NBL depth as a function of U_{starN} for assumed linear and quadratic profiles.

sensible heat flux and a somewhat smaller NBL strength, giving a deeper NBL in the coupled system.

[24] *Monteith* [1981] noted the importance of the velocity scale (16) in surface energy transfer. He defined the reciprocal, $\rho C_p \lambda_0$, as the resistance to longwave radiative transfer. His analysis however focused primarily on the daytime BL. *Nieuwstadt* [1980] derived a rate equation for NBL depth, related to the surface heat flux and cooling rate. He did not use the surface LW_{net} as a scaling parameter, but instead related the radiative cooling rate to the surface cooling rate with an undetermined coefficient, noting that NBL growth solutions depended on his radiation parameterization.

4.3. Nighttime Rise of CO_2 From Respiration

[25] This simple model can be used to estimate the nocturnal rise of other gases that are emitted at the surface and trapped within the NBL. If we confine the CO_2 from respiration at night in a similar way within the NBL with a profile up to depth **h**, we get the storage balance

$$\mathrm{RESPN}\ \tau_N = \beta\ \Delta CO_{2N}\ \mathbf{h} \tag{19}$$

where RESPN is the nighttime respiration in ppm CO_2 m s^{-1}, and ΔCO_{2N} is the surface increase in surface CO_2 at night above the previous daytime ML. Once again, $\beta = 0.5$, 0.33 for linear and quadratic profiles. Substituting for **h** from (15) gives a corresponding estimate of ΔCO_{2N} (both β and τ_N cancel)

$$\Delta CO_{2N} = (\mathrm{RESPN}/\mathbf{W_R})(\Delta T_{Nsc}/H_{Nsc}) \tag{20a}$$

$$= (\mathrm{RESPN}/\mathbf{W_R})R \tag{20b}$$

Figure 10 shows that the ratio $R = (\Delta T_{Nsc}/H_{Nsc})$ varies weakly with τ_N, but decreases steeply with U_{starN} as the NBL gets deeper. Over the range of U_{starN} from 0.1–0.5 m s^{-1} (corresponding in the model to a range of V_{10N} from roughly 0.8 to 3.6 m s^{-1}), ΔCO_{2N} decreases from 237 to 47 ppm (for $\tau_N = 12$ h) for a typical respiration rate, RESPN = 0.2 ppm CO_2 m s^{-1}, and $\mathbf{W_R} \approx 0.0048$ m s^{-1} as before. For fixed respiration rate, the ratio R can be thought of as the amplifier, which increases the NBL rise of CO_2 by reducing the NBL depth, **h**, in (18a), when the surface wind and wind stress are low.

4.4. Nighttime Rise of Radon From Surface Emission

[26] Radon is produced in the soil from decay of radium at a constant rate, and the rate of emission from the soil is approximately constant. Radon has a decay constant, $L_d = 2.089 * 10^{-6}\ s^{-1}$ (corresponding to its half life of 3.8 days), so typical concentrations of radon in the free troposphere are small, about 0.4 Bq m^3 at STP (standard temperature and pressure), and 1.8–3.7 Bq m^3 in the daytime mixed layer [*Kritz et al.*, 1998]. However, in the NBL, radon accumulates and the fraction that decays as the NBL grows is small, as it depends on the product $\tau_N L_d \approx 0.09$, for τ_N =12 h. If this small nocturnal decay term is neglected, the nighttime rise of surface radon, ΔRn_N, is approximately given by

$$\Delta Rn_N \approx (F_{Rn}/\mathbf{W_R})R \tag{21}$$

Over the same range of U_{star} from 0.1–0.5 m s^{-1}, ΔRn_N decreases from 24.9 to 4.9 Bq m^{-3} for a typical emission rate, F_{Rn} = 0.021 Bq m^{-2} s^{-1}. A more exact calculation of the decay loss requires the mixed layer radon at the time when the NBL first forms and decouples from the layer above.

5. Conclusions

[27] This paper proposes a model for the strength and depth of the warm season NBL based on radiative scaling

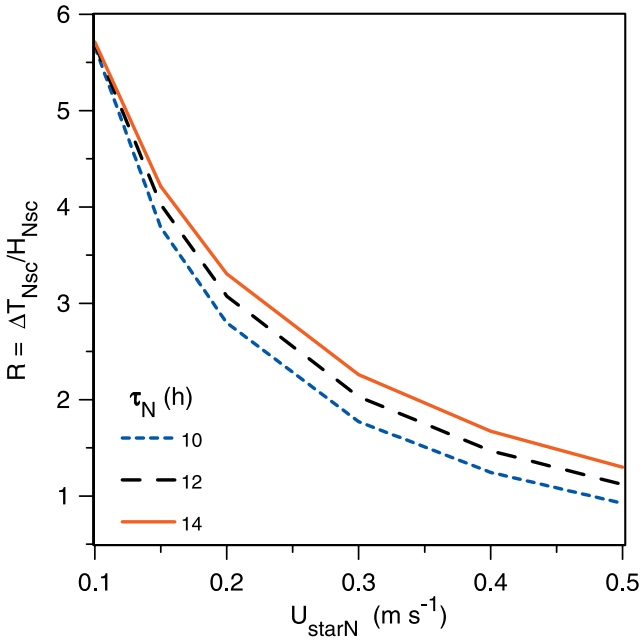

Figure 10. Ratio of scaled NBL strength to scaled heat flux from equation (18b) as a function of U_{starN}.

by the outgoing net longwave flux. This framework differs from the traditional similarity approach to modeling the stable BL in that it emphasizes the primary role of the nocturnal radiative cooling in generating and maintaining a stable structure at night. Historically, comparatively little attention has been paid to the importance of radiative forcing in determining the strength and depth of the NBL. This analysis shows that the strength of the NBL at sunrise, defined here as ΔT_N, and the diurnal temperature range, DTR, are both related to the radiative temperature scale, ΔT_R, derived from the LW_{net} and the slope of the Stefan-Boltzmann equation. Hourly reanalysis data from ERA-40, averaged over river basins, is used to illustrate the scaling, and extract quantitative relationships using multiple linear regression. When scaled by ΔT_R, ΔT_{Nsc} and DTR_{sc} increase with the length of the nighttime stable period and decrease weakly with surface wind stress. The ratio $\Delta T_{Nsc}/DTR_{sc} \approx 0.9 \pm 0.07$. The scaled heat flux increases steeply with wind stress, which controls the strength of the coupling between surface and atmosphere, and the partition between sensible heat flux and ground heat flux. From the NBL energy budget, a simple model for the depth, **h**, of the NBL was then developed in terms of a radiative velocity scale and the scaled surface heat flux, which depends primarily on wind stress. Since increasing wind stress gives a larger sensible heat flux and a somewhat smaller NBL strength, the result in the coupled system is that the depth of the NBL at sunrise increases steeply with wind stress. This simple model for NBL depth was used to estimate the amplification of the nocturnal rise in concentration of CO_2 and radon, that are emitted at the surface.

[28] Numerically, the results are specific to this reanalysis model, ERA-40, and its stable BL and ground heat flux parameterizations, documented in *Viterbo et al.* [1999]. In addition, the analysis has focused on the warm season. However, since both DTR and ΔT_N are observables, this analysis framework can be used to assess the model coupling parameters at the surface (to the atmosphere and to the ground). The model suggests that the DTR, an important climate parameter, is a useful linear measure of the mean surface LW_{net}. The analysis here used the 24-h mean LW_{net} as a scaling parameter for the NBL (as in *Betts*, 2004). The measurement of nighttime surface fluxes, such as H_N is however challenging observationally.

[29] This paper has focused on the growth of the NBL at night in the warm season, and shown also that the DTR is closely related to the strength of the NBL. It might seem surprising that the daytime processes only appear in the analysis through LW_{net24}. For example, *Durre and Wallace* [2001] have shown the impact of evapotranspiration in reducing the DTR during the growing season. *Betts and Viterbo* [2005] showed, for the Madeira subbasin of the Amazon, that diurnally averaged LW_{net24} is related in ERA-40 to both cloud cover and the mean depth of the mixed layer (which is also related to the DTR), and to mean evaporative fraction, itself linked in the model to soil water. In the model, all these processes and the entire diurnal behavior are coupled on the daily timescale, with the result that DTR and ΔT_N have a close relationship to LW_{net24}.

[30] **Acknowledgments.** A. Betts acknowledges support from NSF under grant ATM0529797, from NASA under NEWS grant NNG05GQ88A, and from ECMWF for travel. I am grateful to A. Beljaars and P. Viterbo for helpful discussions and to the entire ERA-40 team for their assistance. Suggestions from two reviewers have significantly improved the paper.

References

Betts, A. K. (1973), Non-precipitating convection and its parameterization, *Q. J. R. Meteorol. Soc.*, *99*, 178–196.

Betts, A. K. (2003), The diurnal cycle over land, in *Forests at the Land-Atmosphere Interface*, edited by M. Mencuccini, J. Grace, J. Moncrieff, and K. McNaughton, pp. 73–93, CABI, Wallingford, U. K.

Betts, A. K. (2004), Understanding hydrometeorology using global models, *Bull. Am. Meteorol. Soc.*, *85*, 1673–1688.

Betts, A. K., and P. Viterbo (2005), Land-surface, boundary layer, and cloud-field coupling over the southwestern Amazon in ERA-40, *J. Geophys. Res.*, *110*, D14108, doi:10.1029/2004JD005702.

Betts, A. K., J. H. Ball, and P. Viterbo (2003), Evaluation of the ERA-40 surface water budget and surface temperature for the Mackenzie River basin, *J. Hydrometeorol.*, *4*, 1194–1211.

Betts, A. K., J. H. Ball, P. Viterbo, A. Dai, and J. A. Marengo (2005), Hydrometeorology of the Amazon in ERA-40, *J. Hydrometeorol.*, *6*, 764–774.

Carson, D. J. (1973), The development of a dry inversion-capped convectively unstable boundary layer, *Q. J. R. Meteorol. Soc.*, *99*, 450–467.

Dai, A., K. E. Trenberth, and T. R. Karl (1999), Effects of clouds, soil moisture, precipitation and water vapor on diurnal temperature range, *J. Clim.*, *12*, 2451–2473.

Deardorff, J. W., G. E. Willis, and D. K. Lilly (1969), Laboratory investigation of non-steady penetrative convection, *J. Fluid Mech.*, *35*, 7–32.

Derbyshire, S. H. (1994), A "balanced" approach to stable boundary layer dynamics, *J. Atmos. Sci.*, *51*, 3486–3504.

Dessens, J., and A. Bucher (1995), Changes in minimum and maximum temperatures at the Pic du Midi in relation with humidity and cloudiness, *Atmos. Res.*, *37*, 147–162.

Durre, I., and J. M. Wallace (2001), The warm season dip in diurnal temperature range over the eastern United States, *J. Clim.*, *14*, 354–360.

Easterling, D. R., et al. (1997), Maximum and minimum temperature trends for the globe, *Science*, *277*, 364–367.

Henderson-Sellers, A. (1992), Continental cloudiness changes this century, *Geol. J.*, *27*, 255–262.

Holtslag, A. A. M., and H. A. R. De Bruin (1988), Applied modeling of the nighttime surface energy balance over land, *J. Appl. Meteorol.*, *27*, 689–704.

Horton, E. B. (1995), The geographical distribution of changes of maximum and minimum temperatures, *Atmos. Res.*, *37*, 101–117.

Jones, P. D. (1995), Maximum and minimum temperature trends in Ireland, Italy, Thailand and Turkey, *Atmos. Res.*, *37*, 67–78.

Kållberg, P., A. Simmons, S. Uppala, and M. Fuentes (2004), The ERA-40 archive, *ERA-40 Proj. Rep. 17*, 31 pp., Eur. Cent. for Medium-Range Weather Forecasts, Reading, U. K.

Karl, T. R., et al. (1993), Asymmetric trends of daily maximum and minimum temperature, *Bull. Am. Meteorol. Soc.*, *74*, 1007–1023.

Kritz, M. A., S. W. Rosner, and D. Z. Stockwell (1998), Validation of an off-line three-dimensional chemical transport model using radon profiles: 1. Observations, *J. Geophys., Res.*, *103*, 8425–8432.

Lilly, D. K. (1968), Models of cloud-topped mixed layers under a strong inversion, *Q. J. R. Meteorol. Soc.*, *94*, 292–309.

Monteith, J. L. (1981), Evaporation and surface temperature, *Q. J. R. Meteorol. Soc.*, *107*, 1–27.

Nieuwstadt, F. T. M. (1980), A rate equation for the inversion height in a nocturnal boundary layer, *J. Appl. Meteorol.*, *19*, 1445–1447.

Nieuwstadt, F. T. M. (1984), The turbulent structure of the stable, nocturnal boundary layer, *J. Atmos. Sci.*, *41*, 2202–2216.

Stull, R. B. (1988), *An Introduction to Boundary Layer Meteorology*, chap. 9, 666 pp., Springer, New York.

Tennekes, H. (1973), A model for the dynamics of the inversion above a convective boundary layer, *J. Atmos. Sci.*, *30*, 558–567.

Uppala, S. M., et al. (2005), The ERA-40 Reanalysis, *Q. J. R. Meteorol. Soc*, *131*, 2961–3012.

Viterbo, P., A. C. M. Beljaars, J.-F. Mahfouf, and J. Teixeira (1999), The representation of soil moisture freezing and its impact on the stable boundary layer, *Q. J. R. Meteorol. Soc.*, *125*, 2401–2426.

A. K. Betts, Atmospheric Research, 58 Hendee Lane, Pittsford, VT 05763, USA. (akbetts@aol.com)